

Dephasing-assisted transport in linear triple quantum dots

L. D. Contreras-Pulido, M. Bruderer, S. F. Huelga, and M. B. Plenio

Institute of Theoretical Physics, Ulm University, D-89069 Ulm, Germany and

Center for Integrated Quantum Science and Technology, Ulm University, D-89069 Ulm, Germany

(Dated: December 6, 2024)

Environmental noise usually hinders the efficiency of charge transport through coherent quantum systems; an exception is dephasing-assisted transport (DAT). We show that linear triple quantum dots in a transport configuration and subjected to local pure dephasing exhibit DAT if the coupling to the drain reservoir exceeds a threshold. DAT occurs for arbitrarily weak dephasing and the enhancement can be directly controlled by the coupling to the drain. Moreover, for specific settings, the enhanced current is accompanied by a reduction in relative shot noise. We identify the quantum Zeno effect and long-distance tunnelling as underlying dynamical processes involved in dephasing-assisted and -suppressed transport. Our analytical results are obtained by using the density matrix formalism and the characteristic polynomial approach to full counting statistics.

PACS numbers: 73.63.Kv, 72.70.+m, 03.65.Yz

I. INTRODUCTION

The presence of environmental noise is generally considered to be an unavoidable hindrance to efficient transport of charge or energy through quantum systems. The general view is that transport in quantum systems relies on their coherence which is inevitably reduced by interactions with an external noisy environment. However, recently environmental noise has been found to play a positive role in transport. Motivated by experiments showing the presence of quantum beating in photosynthetic systems,^{1–3} subsequent theoretical work pointed out that the efficiency of the excitation energy transfer in light-harvesting complexes during photosynthesis can benefit from the presence of environmental noise.^{4–7} The positive influence of dephasing on the transport efficiency, known as dephasing-assisted transport (DAT), was identified as one of the fundamental mechanisms involved.

For achieving a better understanding of this mechanism it is therefore very desirable to implement and explore DAT in the laboratory under controlled conditions. Several proposals in this direction have been made, including transport through quantum optical systems,⁸ information transmission in quantum information platforms,⁹ and heat transport through trapped-ion crystals.¹⁰ The problem of dephasing-enhanced transport in strongly interacting systems has been recently explored for a linear chain of interacting fermions.^{11,12}

In this work we show that the remarkable degree of control achievable in linear triple quantum dots (TQDs) make them well suited for observing DAT and the characteristic current fluctuations associated with it. The linear TQD is composed of tunnel-coupled single-level quantum dots (QDs), depicted schematically in Fig. 1. The first and last QDs are coupled to the source and drain reservoirs, respectively, and pure dephasing acts locally on each QD. We determine analytically several non-equilibrium steady-state properties of the TQD, including the current, shot noise and the coherences of the reduced density matrix.

From our results emerges the following picture: DAT occurs for sufficiently strong coupling to the drain and finite detuning of the central QD. In terms of the energy levels of the TQD, dephasing enhanced transport results from the interplay

between two mechanisms for level-broadening, namely pure dephasing and coupling to the reservoirs. From a dynamic point of view, we argue that the equivalent of the quantum Zeno effect in quantum transport^{13,14} is involved in the occurrence of DAT as an underlying process. Indeed, strong coupling to the drain traps the coherent evolution of the charge between QD1 and QD2, thereby creating a transport bottleneck. The positive impact of dephasing, even if of vanishingly small strength, is to impair this coherent evolution and hence to alleviate the transport bottleneck. Therefore, DAT in the linear TQD with a single excess charge is not due to interference effects, which may originate from geometry, disorder or spin degrees of freedom.^{15–17}

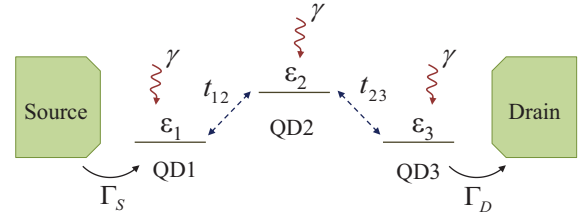


FIG. 1. Three quantum dots with tunnelling couplings t_{ij} are connected to a source (drain) reservoir with rates Γ_S (Γ_D). Local pure dephasing with equal strength γ acts on the single-electron energy levels ε_i . The central quantum dot (QD2) is detuned from the outer dots (QD1 and QD3). The current through the triple quantum dot is brought into the regime of dephasing-assisted transport by increasing the coupling Γ_D above a threshold Γ_D^* .

We also investigate the shot noise of the current to fully explore the existing experimental possibilities of QDs. The problem of fluctuations in TQDs has been addressed for triangular configurations, e.g., in Refs. 18–20. For the linear TQD we find that dephasing-enhanced currents exhibits smaller relative fluctuations, i.e., a larger current-to-noise ratio, than the current without dephasing, at least for experimentally relevant parameter regimes.

Our proposal relies largely on the fact that the experimental study of TQDs emerged recently, uncovering a variety of coherent transport properties.^{21–27} In triangular geometries,

entanglement²⁸ and effects of interference^{15,20,29–31} have been studied, whereas in linear configurations phonon- and photon-assisted transitions as well as the influence of spin-orbit interactions have been analyzed.^{32,33} Most relevant for our proposal, transport measurements in a linear TQD have demonstrated superexchange, i.e., coherent long-distance tunnelling that goes beyond nearest-neighbor quantum dots.^{17,34–36}

Dephasing in quantum dots can be due to background charge noise,^{37–39} inherent electron-phonon interactions^{39–42} or capacitive coupling to a nearby charge detector.^{43–46} Although these interactions are generally accompanied by relaxation processes, dephasing dominates as long as the overlap between wave functions of different local electronic states is small.^{38,40–42} To ensure that environmental effects are dominated by pure dephasing, we detune the central QD significantly, thereby arranging the system in either a Λ -type or V -type configuration [cf. Fig. 1] with mostly localized electronic states. We expect electron-phonon interactions to be the main source of dephasing so that the dephasing rate γ can be controlled via the temperature of the environment in the sub-Kelvin regime. As we focus our interest on the effect of dephasing on transport we refer to Refs. 41, 42, and 47 for microscopical aspects of electron-phonon interactions.

The paper is organized as follows: In Sec. II we define the model in terms of a Lindblad master equation that describes the dynamics of the TQD. Then in Sec. III we present our results: Sec. III A contains a general overview of the transport properties of the TQD, including the exact conditions for the occurrence of DAT. Sec. III B contains an analysis of the dephasing-induced change of the overall coherence of the TQD as well as of the elements of the steady-state density matrix. In Sec. IV we discuss the physical mechanisms relevant for transport (quantum Zeno effect and long-distance tunnelling) in detail, and in Sec. V we suggest an experimental procedure for detecting dephasing-assisted currents. We end with the conclusions in Sec. VI.

II. MODEL AND METHOD

The linear TQD is composed of three tunnel-coupled single-level quantum dots, denoted by QD1, QD2 and QD3, where QD1 and QD3 are coupled to the source and drain reservoirs, respectively [cf. Fig. 1]. We work in the limit of infinite bias voltage and assume that the system is in the Coulomb blockaded regime (the intra-dot Coulomb interaction energy U being the largest energy scale), such that there is at most one extra electron in the TQD. The relevant basis states are accordingly the empty state $|0\rangle$ and the states $|1\rangle$, $|2\rangle$ and $|3\rangle$, in which one of the dots is occupied by a single spinless electron.

The Hamiltonian for the coherent evolution of the TQD is

$$H = (t_{12}d_2^\dagger d_1 + t_{23}d_3^\dagger d_2 + \text{h.c.}) + \sum_i \varepsilon_i d_i^\dagger d_i, \quad (1)$$

where ε_i denotes the on-site energy of an electron on each QD and t_{ij} is the tunnelling coupling between adjacent QDs. The operators d_i^\dagger (d_i) create (annihilate) an electron in the i th QD.

The state of the open system, including reservoirs and environment-induced dephasing, is described by the reduced density matrix $\rho(t)$ of the TQD whose time evolution is governed by the Lindblad master equation^{48,49}

$$\frac{d}{dt}\rho(t) = \mathcal{L}\rho(t) = (\mathcal{L}_c + \mathcal{L}_S + \mathcal{L}_D + \mathcal{L}_\phi)\rho(t). \quad (2)$$

The different Lindblad operators act on $\rho(t)$ as

$$\begin{aligned} \mathcal{L}_c\rho(t) &= -i[H, \rho(t)], \\ \mathcal{L}_S\rho(t) &= \frac{\Gamma_S}{2}(2d_1^\dagger\rho(t)d_1 - \{d_1^\dagger, \rho(t)\}), \\ \mathcal{L}_D\rho(t) &= \frac{\Gamma_D}{2}(2d_3\rho(t)d_3^\dagger - \{d_3^\dagger, \rho(t)\}), \\ \mathcal{L}_\phi\rho(t) &= \frac{\gamma}{2}\sum_i (2n_i\rho(t)n_i - \{n_i, \rho(t)\}), \end{aligned} \quad (3)$$

where $n_i = d_i^\dagger d_i$ and $\{, \}$ stands for the anticommutator. The operator \mathcal{L}_c describes the coherent evolution of the system, while \mathcal{L}_S and \mathcal{L}_D model the irreversible tunnelling of electrons out of the source and into the drain with rates Γ_S and Γ_D , respectively. These rates are energy independent in the wide-band approximation and infinite bias limit. Finally, \mathcal{L}_ϕ describes pure dephasing acting on all three QDs with equal strength. Dephasing causes an exponential decay of the non-diagonal elements of $\rho(t)$ with the rate γ .

We are mainly interested in the regime of small dephasing $\gamma \lesssim t_{ij}$ for two reasons: First, values of this order are typically observed in experiments on lateral coupled QDs.³⁷ Second, if the dephasing rate γ approaches the inter- and intradot Coulomb interaction, then the resulting level-broadening leads to a substantial overlap between the single particle states $\{|1\rangle, |2\rangle, |3\rangle\}$ and higher energy levels of the TQD, which are neglected here; hence we assume $\gamma \ll U$ for consistency. In addition, as shown in experiments,³⁷ variations of the on-site energies ε_i lead to a modification of the dephasing rate γ ; the energies ε_i are therefore held constant.

The influence of dephasing on the steady-state transport through the TQD is analyzed by two measurable quantities, the average current I and the zero-frequency shot noise S . More generally, we consider the probability distribution $p(n)$ of the number n of electrons that tunnel into to the drain within a sufficiently long time interval $\Delta\tau$. We use the characteristic polynomial approach⁵⁰ to determine the full counting statistics, i.e., the distribution $p(n)$, which is parametrized in terms of its cumulants C_k . The essential steps of this approach are briefly outlined in Appendix A. From the time-scaled cumulants $c_k = C_k/\Delta\tau$, we obtain the average current $I = ec_1$ and the shot noise $S = 2e^2c_2$, with e the electron charge. The Fano factor $F = S/2eI$ indicates if the distribution $p(n)$ is sub-Poissonian ($F < 1$) or super-Poissonian ($F > 1$) and gives a measure for the relative shot noise of the current.

III. DEPHASING-ASSISTED TRANSPORT

We first present the results for the transport properties of the TQD in terms of the current I , shot noise S and Fano factor

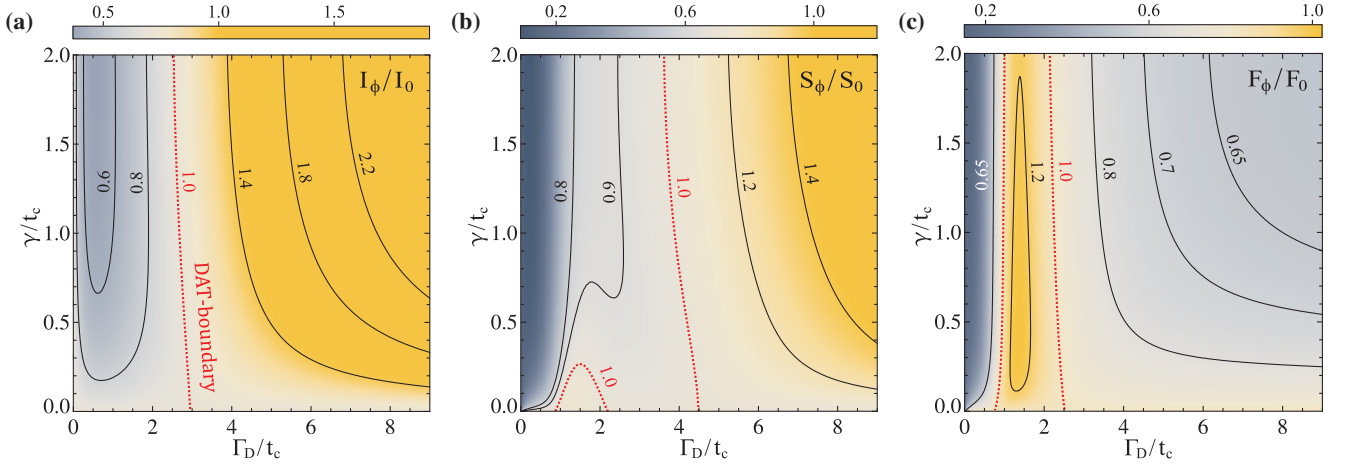


FIG. 2. The effect of dephasing on transport across the TQD for different dephasing rates γ and couplings to the drain Γ_D . **(a)** The ratio I_ϕ/I_0 of the currents with I_ϕ and without I_0 dephasing. The current is enhanced by dephasing ($I_\phi/I_0 > 1$) for Γ_D above the threshold $\Gamma_D^*/t_c \approx 3$. The boundary of the region with DAT ($I_\phi/I_0 = 1$) is given by Eq. (6). The ratios of **(b)** the shot noise S_ϕ/S_0 and **(c)** the Fano factor F_ϕ/F_0 corresponding to **(a)**. Here, the enhanced current is accompanied by a reduced Fano factor, as seen in **(c)**. ($\Gamma_S/t_c = 1/2$ and $\varepsilon/t_c = 4$)

F , and subsequently discuss the properties of the steady-state density matrix ρ^s of the TQD. The characteristic polynomial approach allows us to obtain the transport properties for the most general configuration of the TQD. However, for clarity, we assume for the rest of the paper that the tunnel couplings between the QDs are identical ($t_{12} = t_{23} = t_c$) and that QD1 and QD3 are in resonance ($\varepsilon_1 = \varepsilon_3$). The detuning $\varepsilon = |\varepsilon_1 - \varepsilon_2|$ between the central and outer dots, identical for the Λ -type and V -type configuration, is then sufficient to parametrize the on-site energies ε_i .

A. Dephasing-assisted current and shot noise

The analytical result for the current across the TQD including dephasing is

$$I_\phi = \frac{2et_c^2\Gamma_S\Gamma_D[\gamma\Gamma_\phi^2 + 2t_c^2(4\gamma + \Gamma_D)]}{D_1 + D_2D_3}, \quad (4)$$

where the denominator is composed of

$$\begin{aligned} D_1 &= \Gamma_S\Gamma_D\Gamma_\phi(6\gamma + \Gamma_D)\varepsilon^2, \\ D_2 &= \gamma\Gamma_\phi^2 + 2t_c^2(4\gamma + \Gamma_D), \\ D_3 &= \Gamma_S\Gamma_D(3\gamma + \Gamma_D) + 2t_c^2(3\Gamma_S + \Gamma_D), \end{aligned} \quad (5)$$

with the rate $\Gamma_\phi = 2\gamma + \Gamma_D$. The analytical expression for the shot noise S_ϕ is rather lengthy and therefore given in Appendix B. In the following we explore the physical content of the analytical results.

To identify the parameter regime in which DAT occurs we consider the ratio between the current with dephasing I_ϕ and without dephasing I_0 , the latter being an idealization for negligible dephasing rates. The ratio I_ϕ/I_0 depends only weakly on Γ_S and the detuning ε is kept constant. We therefore map out I_ϕ/I_0 as function of Γ_D and γ for representative values of Γ_S and ε , with all parameters in units of t_c .

Fig. 2(a) shows the typical behaviour of I_ϕ/I_0 . We see that the current is significantly enhanced by dephasing for sufficiently large values of Γ_D . More precisely, the γ - Γ_D plane is divided into two complementary regions, in which the current is either enhanced or suppressed by dephasing. The boundary separating the two regions, defined by $I_\phi/I_0 = 1$, is determined by the relation

$$\varepsilon = \sqrt{6}t_c \left[\frac{\gamma(2\gamma + \Gamma_D)^2 + 2t_c^2(4\gamma + \Gamma_D)}{\Gamma_D(2\gamma + \Gamma_D)^2 - 8t_c^2(3\gamma + \Gamma_D)} \right]^{1/2}. \quad (6)$$

We observe that Eq. (6) does not depend on Γ_S and therefore completely defines the DAT-boundary in the entire parameter space of the system. Moreover, for fixed detuning ε and dephasing γ , we find that Eq. (6) defines a threshold Γ_D^* for dephasing enhanced transport, i.e., DAT is only possible if the coupling Γ_D exceeds the value Γ_D^* . As it can be seen in Fig. 2(a), the dependence of the threshold Γ_D^* on the dephasing γ is rather weak.

It is instructive to examine the regime of weak dephasing $\gamma \ll t_c$, which yields particularly transparent results. Expanding I_ϕ/I_0 to lowest order in γ we find

$$\frac{I_\phi}{I_0} = 1 + \frac{\Gamma_S\Gamma_D[\varepsilon^2(\Gamma_D^2 - 8t_c^2) - 12t_c^4]}{8t_c^6(3\Gamma_S + \Gamma_D) + 2\Gamma_S\Gamma_D^2t_c^2(2t_c^2 + \varepsilon^2)}\gamma. \quad (7)$$

The prefactor of γ can take positive or negative values. Thus, the TQD can be brought into the regime of enhanced transport even for arbitrarily small dephasing γ by tuning the remaining parameters. For weak dephasing, we obtain the simple relation $\varepsilon = 2\sqrt{3}t_c^2/\sqrt{\Gamma_D^2 - 8t_c^2}$ for the DAT-boundary and the corresponding threshold $\Gamma_D^* = 2t_c\sqrt{3t_c^2 + 2\varepsilon^2}/\varepsilon$, both independent of γ . This explicit expression for Γ_D^* shows that finite detuning $\varepsilon > 0$ is necessary for DAT as $\Gamma_D^* \rightarrow \infty$ in the limit $\varepsilon \rightarrow 0$. On the other hand, in the limit of very large level detuning $\varepsilon \rightarrow \infty$ the minimum value for the threshold $\Gamma_D^* = 2\sqrt{2}t_c$ is obtained.

More information about the transport properties of the TQD is encoded in the shot noise S . In particular, the question arises whether or not the dephasing-assisted current comes at the price of an increased level of shot noise. Figs. 2(b) and 2(c) show the ratio of the shot noise S_ϕ/S_0 and the Fano factor F_ϕ/F_0 corresponding to the current I_ϕ/I_0 in Fig. 2(a). We see that dephasing partly enhances the shot noise S_ϕ/S_0 in the DAT region; however, the level of noise relative to the current, quantified by F_ϕ/F_0 , is reduced.

In general, the shot noise corresponding to the dephasing-assisted current depends in an intricate way on the parameters of the system, and both dephasing-increased and -suppressed relative shot noise may be found. To have a better understanding of the fluctuations of the current, we consider the two specific cases of vanishingly small coupling $\Gamma_S \rightarrow 0$ and large coupling $\Gamma_S \gg t_c$ to the source. In the former limit, we expand F_ϕ/F_0 to lowest order in Γ_S to find

$$\frac{F_\phi}{F_0} = 1 - \left[\frac{3\gamma}{t_c^2} + \frac{\gamma\epsilon^2(24\gamma t_c^2 + 8\Gamma_D t_c^2 - \Gamma_D \Gamma_\phi^2)}{2t_c^4(8\gamma t_c^2 + 2\Gamma_D t_c^2 + \gamma\Gamma_\phi^2)} \right] \Gamma_S. \quad (8)$$

From Eq. (8) we determine the boundary between enhanced and suppressed relative shot noise, defined by $F_\phi/F_0 = 1$. It turns out that this boundary is identical to the DAT-boundary

$$\begin{aligned} \rho_{11}^s &= \frac{\Gamma_S}{2} \frac{2t_c^2(8\gamma^3 + 24\gamma^2\Gamma_D + 10\gamma\Gamma_D^2 + \Gamma_D^3) + 8t_c^4(4\gamma + \Gamma_D) + \Gamma_\phi\Gamma_D(4\gamma + \Gamma_D)(\gamma\Gamma_\phi + 2\epsilon^2)}{D_1 + D_2D_3} \\ \rho_{22}^s &= \frac{\Gamma_S}{2} \frac{2t_c^2\Gamma_\phi(4\gamma^2 + 6\gamma\Gamma_D + \Gamma_D^2) + 8t_c^4(4\gamma + \Gamma_D) + \gamma\Gamma_\phi\Gamma_D(\Gamma_\phi^2 + 4\epsilon^2)}{D_1 + D_2D_3} \\ \rho_{33}^s &= \frac{\Gamma_S}{2} \frac{4t_c^2[\gamma\Gamma_\phi^2 + 2t_c^2(4\gamma + \Gamma_D)]}{D_1 + D_2D_3} \end{aligned} \quad (9)$$

where D_1 , D_2 and D_3 are defined in Eq. (5). The occupation of the empty state ρ_{00}^s , which is typically small but finite, can be found from the normalization condition $\sum_i \rho_{ii}^s = 1$. Note that in our case of infinite bias voltage and strong Coulomb blockade, the steady-state current measured at the drain is given by $I = e\Gamma_D\rho_{33}^s$.

The occupations ρ_{ii}^s for increasing Γ_D with and without dephasing are shown in Fig. 3(a). In accord with the behaviour of the current, dephasing reduces the occupation ρ_{33}^s of QD3 in the regime $\Gamma_D < \Gamma_D^*$, while ρ_{33}^s is dephasing-enhanced in the regime $\Gamma_D > \Gamma_D^*$ where DAT is observed. In the fully coherent case, i.e., in absence of dephasing, both ρ_{11}^s and ρ_{22}^s show signatures of the trapped coherent evolution between QD1 and QD2: For sufficiently large values of Γ_D the occupations ρ_{11}^s and ρ_{22}^s are approximately constant and account for most of the occupation of the TQD. In addition, we observe that $\rho_{22}^s \ll \rho_{11}^s$ as a result of the large detuning ϵ between the QDs, such that the charge is essentially localized in QD1. Dephasing significantly reduces the difference between all occupations ρ_{ii}^s , in particular between ρ_{22}^s and ρ_{11}^s , and consequently counteracts the localization effect. We will

given by Eq. (6) and that enhanced transport is always accompanied by an increased Fano factor in the limit $\Gamma_S \rightarrow 0$.

In the opposite limit $\Gamma_S \gg t_c$, we expand F_ϕ/F_0 to lowest order in Γ_S^{-1} to obtain an expression for the boundary $F_\phi/F_0 = 1$ which is independent of Γ_S . In contrast to the previous case, the DAT region lies inside the region of a reduced Fano factor for all dephasing rates γ , similar to the example shown in Figs. 2(a) and 2(c). Thus, dephasing not only enhances the current through the TQD but also reduces the relative fluctuations in the regime $\Gamma_S \gg t_c$.

B. Occupations and coherences of the reduced density matrix for the TQD

We now turn to a discussion of the steady-state density matrix ρ^s of the TQD, which is determined by solving $\mathcal{L}\rho^s = 0$. The occupations ρ_{ii}^s and especially the coherences between different electronic states $\rho_{i \neq j}^s$ play a crucial role for the transport processes. Unlike the current and shot noise, the density matrix ρ^s is not directly accessible by measurements, yet useful for complementing our previous findings in terms of the dynamics of the TQD.

The occupation probabilities for each state of the TQD including dephasing read

further clarify the behavior of the occupations in context of the quantum Zeno effect in the next section.

The coherences of the TQD are given by

$$\begin{aligned} \rho_{12}^s &= \frac{t_c\Gamma_D\Gamma_S[(\epsilon + i\gamma)\Gamma_\phi^2 + 2it_c^2(4\gamma + \Gamma_D)]}{D_1 + D_2D_3}, \\ \rho_{23}^s &= \frac{it_c\Gamma_D\Gamma_S[2t_c^2(4\gamma + \Gamma_D) + \gamma\Gamma_\phi(\Gamma_\phi + 2i\epsilon)]}{D_1 + D_2D_3}, \\ \rho_{13}^s &= \frac{2i\epsilon t_c^2\Gamma_D\Gamma_S(4\gamma + \Gamma_D)}{D_1 + D_2D_3} \end{aligned} \quad (10)$$

and $\rho_{j0}^s = 0$ for $j \neq 0$. To assess the effect of dephasing on the coherence of the TQD in a quantitative way we use the l_1 -norm⁵¹

$$C(\rho) = \sum_{i \neq j} |\rho_{ij}| \quad (11)$$

as a measure of the overall coherence in the system. Specifically, we analyze the ratio $C(\rho_\phi^s)/C(\rho_0^s)$, shown in Fig. 3(c)

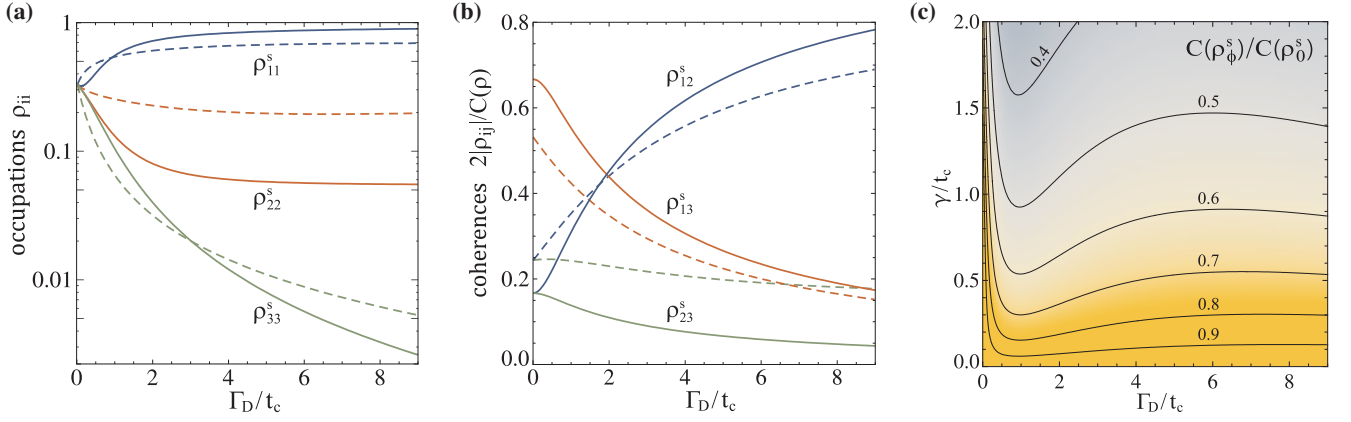


FIG. 3. The effect of dephasing on the properties of the steady-state density matrix ρ^s of the TQD. **(a)** The occupations ρ_{ii}^s as a function of the coupling to the drain Γ_D without (solid line) and with (dashed line) dephasing. Dephasing increases ρ_{33}^s for $\Gamma_D > \Gamma_D^*$ and reduces the difference between ρ_{11}^s and ρ_{22}^s . **(b)** The weights of the coherences ρ_{ij}^s with respect to the overall coherence $C(\rho^s)$. The large weight of ρ_{13}^s for $\Gamma_D \lesssim t_c$ indicates long-distance tunnelling and the dominance of ρ_{12}^s for $\Gamma_D \gg t_c$ is a signature for the quantum Zeno effect. **(c)** The overall coherence of the TQD is specified by the ratio $C(\rho_\phi^s)/C(\rho_0^s)$ of the l_1 -norm of coherence. Even moderate dephasing rates γ reduce the coherence considerably. There is no relation apparent between the overall coherence and the transport properties in Fig. 2. ($\Gamma_S/t_c = 1/2$, $\varepsilon/t_c = 4$ and $\gamma/t_c = 2/3$)

as a function of Γ_D and γ . As expected, we see that the overall coherence of the TQD is reduced with increasing γ . It is interesting, however, that for constant γ the coherence tends to be higher in the DAT region, which indicates that dephasing enhanced transport is not directly related to a reduction of the overall coherence.

The weights of specific coherences ρ_{ij}^s with respect to the overall coherence $C(\rho)$ are more informative and can be quantified as $2|\rho_{ij}^s|/C(\rho^s)$. This ratio is shown in Fig. 3(b) for the coherences ρ_{13}^s , ρ_{12}^s and ρ_{23}^s with and without dephasing as a function of Γ_D . We see that the coherence ρ_{13}^s , indicating long-distance tunnelling between the outer QDs of the array, accounts for most of the coherence in the regime $\Gamma_D \lesssim t_c$ while ρ_{12}^s is the dominating contribution for $\Gamma_D \gg t_c$. These observations are discussed further in the next section and support our explanations of DAT and suppressed transport based on the quantum Zeno effect and long-distance tunnelling, respectively.

IV. UNDERLYING DYNAMIC PROCESSES

We now focus on the underlying physical processes that account for enhanced and suppressed currents across the system. Transport through the TQD is determined by its energy levels, the tunnel coupling and the effects of the reservoirs. Accordingly, DAT can be explained as a consequence of level-broadening caused by both, pure dephasing and the coupling to the reservoirs. Nevertheless, our previous results suggest that we can also understand DAT in terms of the dynamics of the charge, which yields further insight into the role of dephasing. To this end, we present two effective models for the evolution of the TQD, which involve the equivalent of the quantum Zeno effect in quantum transport^{13,14} and long-distance tunnelling.³⁴⁻³⁶ Both models reduce the problem of the TQD

to an effective double quantum dot (DQD).

A. Quantum Zeno effect

Dephasing-enhanced transport occurs for Γ_D exceeding the threshold Γ_D^* , typically $\Gamma_D \gg t_c$, provided that the detuning ε is finite. To understand the predicted DAT let us first consider the TQD in the fully coherent regime. The coherent evolution of the electrons in the TQD is characterized by the time scale $\tau_c \sim t_c^{-1}$. Moreover, because QD3 is coupled to the drain we have that QD3 is repeatedly emptied, or equivalently observed, on a time scale $\tau_D \sim \Gamma_D^{-1}$, the average time interval between subsequent detections. For sufficiently strong coupling Γ_D , the irreversible tunnelling into the drain can be considered as a continuous measurement of QD3 on a time scale $\tau_D \ll \tau_c$, so that the ensuing Zeno effect restricts the evolution of the charge to QD1 and QD2. In other words, the charge is localized and evolves coherently between QD1 and QD2 only, which is confirmed by the dominance of the coherence ρ_{12}^s in the regime $\Gamma_D \gg t_c$ [cf. Fig. 3(b)].

To be more quantitative, we describe the TQD in the Zeno regime in absence of dephasing by an effective model for QD1 and QD2, whose evolution is governed by

$$H^Z = (t_{12}d_2^\dagger d_1 + \text{h.c.}) + \sum_{i \neq 3} \varepsilon_i^Z d_i^\dagger d_i, \quad (12)$$

$$\mathcal{L}_D^Z \rho = \frac{\Gamma_D^Z}{2} (2d_2 \rho d_2^\dagger - \{d_2^\dagger d_2, \rho\})$$

together with the Lindblad operator \mathcal{L}_S in Eq. (3). The evolution of the charge in this effective DQD is reduced to the subspace spanned by the states $\{|0\rangle, |1\rangle, |2\rangle\}$ and tunnelling into

the drain occurs now from QD2 with the effective rate^{52,53}

$$\Gamma_D^Z = 2t_{23}^2 \frac{\Gamma_D/2}{(\Gamma_D/2)^2 + (\varepsilon_2 - \varepsilon_3)^2}. \quad (13)$$

In addition, the on-site energy of the second QD is shifted to $\varepsilon_2^Z = \varepsilon_2(1 + \Gamma_D^Z/\Gamma_D)$, with however a negligible effect on the transport properties, while ε_1 is unaffected. We note that, alternatively, Eqs. (12) and (13) can be interpreted as a strong Lorentzian level broadening of QD3 due to the coupling to the drain with the corresponding reduction of the local spectral density. The effective Zeno model is valid in the regime $\Gamma_D \gg t_c$ and $\gamma = 0$, where it reproduces the behaviour of the current through the TQD, as shown in Appendix C.

Importantly, the current is strongly suppressed as the dynamics approaches the Zeno regime, according to Eq. (13), because the effective coupling to the drain $\Gamma_D^Z \ll \Gamma_D$ constitutes a transport bottleneck. We also point out the essential fact that the Zeno effect relies on the coherent evolution of the TQD. Therefore, the transport bottleneck is not expected to occur for incoherent transport between the QDs.

The role of dephasing is to impair the coherence of the TQD and hence to render the Zeno effect less efficient. In fact, dephasing reduces the trapped coherent evolution between QD1 and QD2, resulting in the reduction of the coherence ρ_{12}^s [cf. Fig. 3(b)], and generally enables incoherent transitions between all QDs. In this way, dephasing partially alleviates the transport bottleneck and consequently the dephasing-assisted current arises. This is reflected, also, in the change of the occupations ρ_{ii}^s due to the presence of dephasing, as specifically ρ_{11}^s is reduced while ρ_{22}^s and ρ_{33}^s are increased for finite γ [cf. Fig. 3(a)].

B. Long-distance tunnelling

The suppression of the current for $\Gamma_D \lesssim t_c$, as seen in Fig. 2(a), can be understood in terms of the long-distance tunnelling between QD1 and QD3. For the large detuning ε of the central QD, long-distance tunnelling provides the dominant mechanism for charge transport through the TQD. The effect of dephasing is to destruct this coherent pathway, leading to a suppressed current.

In order to have a better understanding of the negative impact of dephasing, we use an effective model for QD1 and QD3. In the coherent regime and for large detuning $\varepsilon \gg t_c$ we can eliminate the state $|2\rangle$ from the dynamics of the TQD, leaving us with an effective DQD described by

$$H^{\text{ld}} = (t_{13}^{\text{ld}} d_3^\dagger d_1 + \text{h.c.}) + \sum_{i \neq 2} \varepsilon_i^{\text{ld}} d_i^\dagger d_i \quad (14)$$

together with the Lindblad operators \mathcal{L}_S , \mathcal{L}_D and \mathcal{L}_ϕ in Eq. (3). Here, t_{13}^{ld} is the effective long-distance tunnelling between QD1 and QD3, $\varepsilon_i^{\text{ld}}$ are renormalized on-site energies and the parameters entering \mathcal{L}_S , \mathcal{L}_D and \mathcal{L}_ϕ are replaced by their effective counterparts Γ_S^{ld} , Γ_D^{ld} and γ^{ld} . Note

that the evolution of the charge is reduced now to the subspace spanned by the states $\{|0\rangle, |1\rangle, |3\rangle\}$. The effective long-distance model reproduces the current across the TQD for $\gamma = 0$ and $\Gamma_D \lesssim t_c$, as shown in Appendix D, where we used $t_{13}^{\text{ld}} = (\varepsilon - \sqrt{\varepsilon^2 + 8t_c^2})/4$ obtained from an improved adiabatic elimination method.⁵⁴

In general, for this effective DQD we find that dephasing always leads to a suppression of the current provided that $\varepsilon_1^{\text{ld}} = \varepsilon_3^{\text{ld}}$, as in this case (Appendix D)

$$\frac{I_\phi^{\text{ld}}}{I_0^{\text{ld}}} = 1 - \frac{2\gamma^{\text{ld}}\Gamma_S^{\text{ld}}\Gamma_D^{\text{ld}}}{\Gamma_S^{\text{ld}}\Gamma_D^{\text{ld}}(2\gamma^{\text{ld}} + \Gamma_D^{\text{ld}}) + (2t_{13}^{\text{ld}})^2(2\Gamma_S^{\text{ld}} + \Gamma_D^{\text{ld}})} \quad (15)$$

so that indeed $I_\phi^{\text{ld}}/I_0^{\text{ld}} \leq 1$. This result, which is independent of the details of the effective model, explains the suppressed current of the TQD in regimes where long-distance tunnelling plays an important role in transport. The reduction of the current can be significant even for weak dephasing $\gamma \ll t_c$ as the relevant ratio $\gamma^{\text{ld}}/t_{13}^{\text{ld}}$ may still be large.

V. EXPERIMENTAL IMPLEMENTATION

Let us now discuss how DAT can be unambiguously detected in an experiment. An interesting aspect of transport through the linear TQD is not only that it exhibits DAT but, importantly, that the boundary between suppressed and enhanced transport can be crossed by changing a single external parameter. This crossing provides a clear signature for the observation of DAT.

In order to detect DAT we envisage the following experimental procedure with all parameters based on typical values for lateral QDs:^{34,35,37} The current and shot noise are measured with two different values of the dephasing rate, $\gamma_1 = 1\mu\text{eV}$ and $\gamma_2 = 2.5\mu\text{eV}$. In both measurements, the coupling of QD3 to the drain Γ_D is varied in the range $0 - 30\mu\text{eV}$, while the inter-dot tunnelling coupling $t_c = 5\mu\text{eV}$, the detuning $\varepsilon = 20\mu\text{eV}$ and the coupling to the source $\Gamma_S = 1\mu\text{eV}$ are kept constant. The dephasing rate γ can be modified, for instance, by increasing the temperature of the environment, which results in enhanced electron-phonon interactions.⁴¹ We emphasize that the exact value of the rates γ_1 and γ_2 is not essential for our scheme as long as $\gamma_2 > \gamma_1$, and that the strength of dephasing has not to be identical for all QDs, i.e., unavoidable small fluctuations of the dephasing rate $\delta\gamma \ll \gamma_2 - \gamma_1$ acting on each QD do not affect the overall qualitative results.

Considering the ratio of the measured currents $I_{\gamma_2}/I_{\gamma_1}$ as a function of the coupling to the drain Γ_D , we expect to observe the crossover to DAT close to $\Gamma_D \cong 13.5\mu\text{eV}$, as shown in Fig. 4(a). The shot noise for γ_1 and γ_2 is practically identical in the DAT regime so that the ratio of the Fano factors $F_{\gamma_2}/F_{\gamma_1}$ decreases for the selected parameters. The specific values of the two currents I_{γ_1} and I_{γ_2} , which are more relevant for the experimental implementation, are shown in Fig. 4(b). The currents deviate by approximately 10pA (15%) well inside the regions where transport is either suppressed or enhanced, which is detectable by using standard technologies for lateral quantum dots.

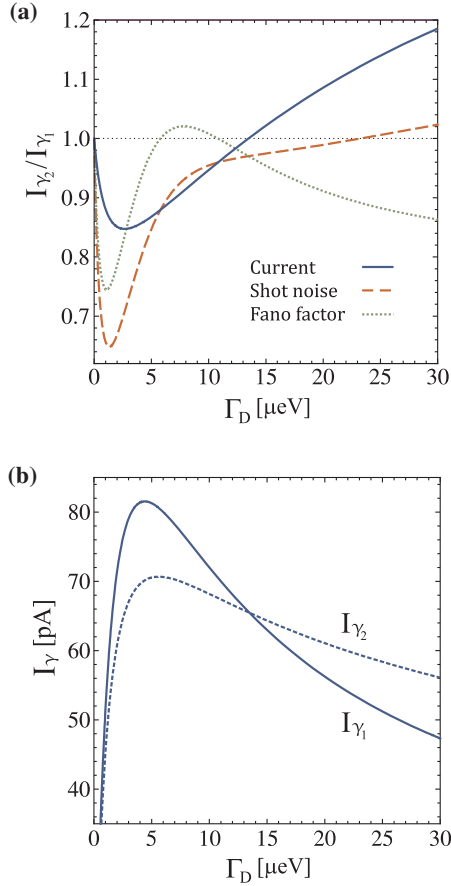


FIG. 4. **(a)** The ratio of the currents $I_{\gamma_2}/I_{\gamma_1}$ (solid line) for two values of the dephasing rate $\gamma_2 > \gamma_1$. For Γ_D exceeding the threshold $\Gamma_D^* \cong 13.5\mu\text{eV}$ we observe dephasing-enhanced transport, i.e., $I_{\gamma_2}/I_{\gamma_1} > 1$. The shot noise $S_{\gamma_2}/S_{\gamma_1}$ (dashed line) increases while the Fano factor $F_{\gamma_2}/F_{\gamma_1}$ (dotted line) decreases in the DAT region. **(b)** The currents I_{γ_1} (solid line) and I_{γ_2} (dashed line) for increasing Γ_D . The crossing at the threshold Γ_D^* provides a clear signature for the detection of DAT. (Parameters in the main text)

VI. CONCLUSIONS

We have proposed a concrete realization of DAT in a highly controllable quantum system. Our comprehensive and fully analytical results demonstrate that dephasing-assisted currents can be observed in linear TQDs in a transport configuration. Moreover, we have suggested an experimental procedure that provides an unambiguous way to verify the occurrence of DAT in controlled conditions.

Specifically, we have found that enhanced transport in linear TQDs occurs for sufficiently strong coupling to the drain and results from the reduction of the quantum Zeno effect, in contrast to triangular TQDs, where destructive interferences are the underlying cause for DAT. We also found that dephasing can suppress the current for moderate coupling to the drain due to the reduction of the long-distance tunnelling between the outer dots of the TQD. Both enhancement and suppression of the current induced by dephasing were shown to be directly reflected in the behavior of the coherences of the reduced den-

sity matrix of the TQD. While the above results have been obtained for a symmetric configuration of the linear TQD our findings are qualitatively valid also for moderately asymmetric configurations, e.g., with slightly different tunneling couplings, $t_{12} \neq t_{23}$. In such a case, significant changes on the transport properties occur only in the regime of vanishingly weak coupling to the drain.

The example of the TQD clearly shows that the coupling to the drain reservoir plays a crucial role in DAT. This general conclusion may be relevant for other transport systems, in particular for larger arrays of QDs. Finally, we have revealed that dephasing induces significant changes in the relative level of shot noise. The underlying mechanisms responsible for these changes and the consequences of this result need yet to be explored.

ACKNOWLEDGMENTS

We are grateful to R. Aguado and G. Platero for helpful discussions and comments. This work has been supported from the ERC Synergy grant BioQ, the EU Integrating project SIQS, the EU STREP project PAPETS and the Alexander von Humboldt Foundation.

VII. APPENDIX

Appendix A: Characteristic polynomial approach

The characteristic polynomial approach to determine the full counting statistics for an open quantum system is explained in detail in Ref. 50. Let us briefly outline here the essential steps of the method. We first transform the original \mathcal{L} into the deformed Lindblad operator $\mathcal{L} \rightarrow \mathcal{L}_\xi$ by making the substitution $d_3 \rho d_3^\dagger \rightarrow e^\xi d_3 \rho d_3^\dagger$ in Eq. (3), thereby introducing the counting variable ξ . We then calculate the characteristic polynomial $P_\xi(x) = \det[x\mathcal{I} - \mathcal{L}_\xi]$ of the deformed operator \mathcal{L}_ξ , where \mathcal{L}_ξ is expressed as a matrix of dimension $M \times M$ and \mathcal{I} is the identity. The characteristic polynomial $P_\xi(x)$ in its coefficient form reads

$$P_\xi(x) = x^M + a_{M-1}x^{M-1} + \sum_{j=0}^{M-2} a_j(\xi)x^j. \quad (\text{A1})$$

The coefficients $a_j = a_j(\xi)|_{\xi=0}$ and their derivatives $a'_j = \partial_\xi a_j(\xi)|_{\xi=0}$ immediately yield the time-scaled cumulants $c_k = C_k/\Delta\tau$ of the distribution $p(n)$. Specifically, we have for the average c_1 , the variance c_2 and the Fano factor F

$$\begin{aligned} c_1 &= -a'_0/a_1, \\ c_2 &= -(a'_0 + 2a'_1c_1 + 2a_2c_1^2)/a_1, \\ F &= c_2/c_1 = 1 + 2(a'_0a_2 - a'_1a_1)/a_1^2. \end{aligned} \quad (\text{A2})$$

From the cumulants we directly obtain analytical expressions for the average current $I = ec_1$ and the zero-frequency shot noise $S = 2e^2c_2$, with e the electron charge.

Appendix B: Transport properties of the triple quantum dot including pure dephasing

To obtain the general expressions for c_1 and c_2 we first construct the matrix of dimension 16×16 corresponding to \mathcal{L}_ξ , determine the characteristic polynomial $P_\xi(x)$ and then make use of Eqs. (A2). The result for the current c_1 is given in the

main text [cf. Eq. (4)]. For the shot noise we find

$$c_2 = \frac{B_1}{B_9} \left(B_2 B_3 + \sum_{i=4}^8 B_i \right), \quad (\text{B1})$$

where the expressions for the B_i are

$$\begin{aligned} B_1 &= 2\Gamma_S \Gamma_D t_c^2 [\gamma \Gamma_\phi^2 + 2t_c^2 (4\gamma + \Gamma_D)], \\ B_2 &= 2\Gamma_S^2 \Gamma_D t_c^2 \Gamma_\phi^2, \\ B_4 &= 16t_c^8 (4\gamma + \Gamma_D)^2 [2\gamma (9\Gamma_S^2 + \Gamma_D^2) + 11\Gamma_S^2 \Gamma_D + \Gamma_D^3], \end{aligned}$$

with the rate $\Gamma_\phi = 2\gamma + \Gamma_D$, and furthermore

$$\begin{aligned} B_3 &= \varepsilon^2 (80\gamma^4 + 264\gamma^3 \Gamma_D + 164\gamma^2 \Gamma_D^2 + 34\gamma \Gamma_D^3 + 3\Gamma_D^4) + \gamma \Gamma_\phi (40\gamma^4 + 92\gamma^3 \Gamma_D + 60\gamma^2 \Gamma_D^2 + 17\gamma \Gamma_D^3 + 2\Gamma_D^4) + 8\gamma \Gamma_D \varepsilon^4, \\ B_5 &= \Gamma_S^2 \Gamma_D^2 \Gamma_\phi^3 [\varepsilon^4 (28\gamma^2 + 8\gamma \Gamma_D + \Gamma_D^2) + \gamma \varepsilon^2 \Gamma_\phi (28\gamma^2 + 14\gamma \Gamma_D + \Gamma_D^2) + \gamma^2 \Gamma_\phi^2 (7\gamma^2 + 5\gamma \Gamma_D + \Gamma_D^2)], \\ B_6 &= 8t_c^6 \Gamma_\phi (4\gamma + \Gamma_D) [8\gamma^3 (9\Gamma_S^2 + \Gamma_D^2) + 8\gamma^2 (15\Gamma_S^2 \Gamma_D + \Gamma_D^3) + 2\gamma (14\Gamma_S^2 \Gamma_D^2 + \Gamma_D^4) - \Gamma_S^2 \Gamma_D (\Gamma_D^2 - 4\varepsilon^2)], \\ B_7 &= 4t_c^4 \Gamma_\phi [16\gamma^6 (9\Gamma_S^2 + \Gamma_D^2) + 16\gamma^5 (39\Gamma_S^2 \Gamma_D + 2\Gamma_D^3) + 24\gamma^4 (30\Gamma_S^2 \Gamma_D^2 + \Gamma_D^4) + \Gamma_S^2 \Gamma_D^4 (\Gamma_D^2 - 4\varepsilon^2)], \\ B_8 &= 4t_c^4 \Gamma_\phi \{ 4\gamma^3 [\Gamma_S^2 (85\Gamma_D^3 + 44\Gamma_D \varepsilon^2) + 2\Gamma_D^5] + \gamma^2 [\Gamma_S^2 (78\Gamma_D^4 + 88\Gamma_D^2 \varepsilon^2) + \Gamma_D^6] + \gamma \Gamma_S^2 \Gamma_D^3 (11\Gamma_D^2 + 4\varepsilon^2) \}, \\ B_9 &= \Gamma_\phi \{ \Gamma_S \Gamma_D \Gamma_\phi \varepsilon^2 (6\gamma + \Gamma_D) + [\gamma \Gamma_\phi^2 + 2t_c^2 (4\gamma + \Gamma_D)] [\Gamma_S \Gamma_D (3\gamma + \Gamma_D) + 2t_c^2 (3\Gamma_S + \Gamma_D)] \}^3. \end{aligned}$$

Appendix C: Effective model for the Zeno-like regime

In the regime $\Gamma_D \gg t_c$, the equivalent of the quantum Zeno effect in quantum transport^{13,14} occurs. This effect reduces the TQD to an effective DQD described by Eq. (12). The current I^Z for the effective DQD is obtained from the known expression for the current across a DQD,⁵⁵ namely by replacing the rate to the drain Γ_D by the effective rate Γ_D^Z in Eq. (13), and reads

$$I^Z = \frac{4\Gamma_S \Gamma_D^Z t_c^2}{4\Gamma_S \varepsilon^2 + \Gamma_S (\Gamma_D^Z)^2 + 4t_c^2 (2\Gamma_S + \Gamma_D^Z)}. \quad (\text{C1})$$

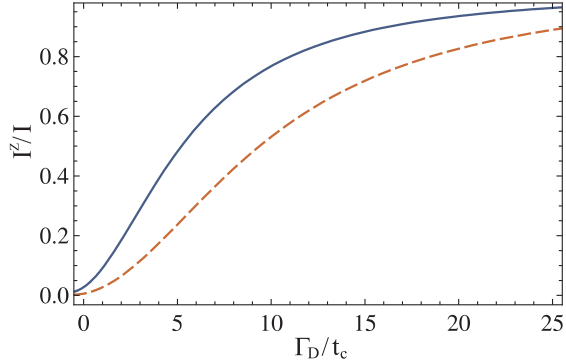


FIG. 5. The ratio I^Z/I for two values of the level detuning, $\varepsilon/t_c = 3$ (solid line) and $\varepsilon/t_c = 5$ (dashed line), showing that the agreement between the effective DQD model, Eq. (12), and the full TQD system is reached for $\Gamma_D \gg t_c$. ($\Gamma_S/t_c = 1/2$)

This effective current I^Z reproduces the average current for the full TQD system I well in the limit $\Gamma_D \gg t_c$, as we can see from the ratio I^Z/I shown in Fig. 5. We note that the ratio I^Z/I approaches the asymptotic value 1 in the full Zeno regime, which is reached for values of Γ_D larger than those explored in Fig. 5. Nevertheless, for the regime of parameters where we predict DAT, the effect of large Γ_D is already partially taking the system to the Zeno regime. This is noticeable by the suppression of the current in absence of dephasing, as seen in Fig. 3(b) for ρ_{33}^s .

Appendix D: Long-distance tunnelling and the effect of pure dephasing on the transport properties of a DQD

In Section IV B we pointed out that in the regime $\varepsilon \gg t_c$ and $\Gamma_D \lesssim t_c$ the long-distance tunnelling between QD1 and QD3 plays a role in the transport across the TQD. We can understand this effect by first considering the TQD in absence of dephasing and decoupled from the reservoirs. For large detuning $\varepsilon \gg t_c$ it is possible to eliminate the central dot and describe the system by an effective DQD composed by QD1 and QD3, with the corresponding Hamiltonian in Eq. (14) and the effective tunnel coupling t_{13}^{ld} between the outer dots.

We include now the coupling to the source and drain reservoirs. Similarly as in Appendix C, the current through the effective system I^{ld} is obtained by replacing the tunnel coupling t_{13}^{ld} and the effective rates Γ_S^{ld} and Γ_D^{ld} in the known expression

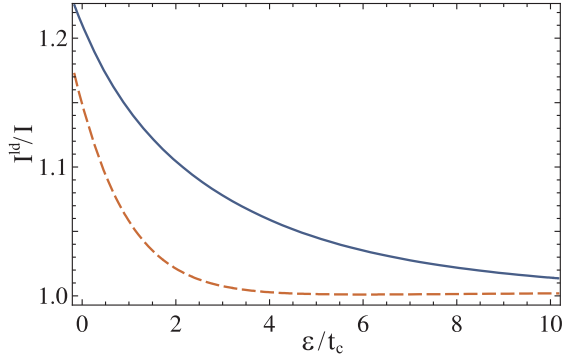


FIG. 6. The ratio I^{ld}/I for two values of the coupling to the drain reservoir, $\Gamma_D/t_c = 1$ (solid line) and $\Gamma_D/t_c = 3/2$ (dashed line), showing the agreement between the effective DQD model for QD1 and QD3, Eq. (14), and the full TQD system in the regime $\varepsilon \gg t_c$. ($\Gamma_S/t_c = 1/2$)

for the current through a DQD, that is

$$I^{\text{ld}} = \frac{4\Gamma_S^{\text{ld}}\Gamma_D^{\text{ld}}(t_{13}^{\text{ld}})^2}{4\Gamma_S^{\text{ld}}(\varepsilon_{13}^{\text{ld}})^2 + \Gamma_S^{\text{ld}}(\Gamma_D^{\text{ld}})^2 + 4(t_{13}^{\text{ld}})^2(2\Gamma_S^{\text{ld}} + \Gamma_D^{\text{ld}})}, \quad (\text{D1})$$

with $\varepsilon_{13}^{\text{ld}} = \varepsilon_1^{\text{ld}} - \varepsilon_3^{\text{ld}}$ and $\varepsilon_i^{\text{ld}}$ the renormalized on-site energies.

In particular, we can follow the procedure in Ref. 54 to adiabatically eliminate the state $|2\rangle$, which yields explicitly $t_{13}^{\text{ld}} = (\varepsilon - \sqrt{\varepsilon^2 + 8t_c^2})/4$ and identical renormalized on-site energies $\varepsilon_1^{\text{ld}} = \varepsilon_3^{\text{ld}}$. Using these expressions together with $\Gamma_{S/D}^{\text{ld}} = \Gamma_{S/D}$ we find that the current I^{ld} reproduces the cur-

$$F_{\phi}^{\text{ld}} = 1 - \frac{8\Gamma_S^{\text{ld}}\Gamma_D^{\text{ld}}(t_{13}^{\text{ld}})^2 \{4(\varepsilon_{13}^{\text{ld}})^2 [2\gamma^{\text{ld}}(\Gamma_S^{\text{ld}} + \Gamma_D^{\text{ld}}) + \Gamma_D^{\text{ld}}(\Gamma_D^{\text{ld}} - \Gamma_S^{\text{ld}})] + (\Gamma_{\phi}^{\text{ld}})^2 [2\gamma^{\text{ld}}(\Gamma_S^{\text{ld}} + \Gamma_D^{\text{ld}}) + \Gamma_D^{\text{ld}}(3\Gamma_S^{\text{ld}} + \Gamma_D^{\text{ld}}) + 8(t_{13}^{\text{ld}})^2]\}}{\{\Gamma_S^{\text{ld}}\Gamma_D^{\text{ld}}[(\Gamma_{\phi}^{\text{ld}})^2 + 4(\varepsilon_{13}^{\text{ld}})^2] + 4(t_{13}^{\text{ld}})^2\Gamma_{\phi}^{\text{ld}}(2\Gamma_S^{\text{ld}} + \Gamma_D^{\text{ld}})\}^2}, \quad (\text{D2})$$

with $\Gamma_{\phi}^{\text{ld}} = 2\gamma^{\text{ld}} + \Gamma_D^{\text{ld}}$. We notice that I_{ϕ}^{ld} in Eq. (D2) is equivalent to the current obtained for a DQD coupled to a bosonic bath within the Born-Markov approximation, if only the contribution of pure dephasing is considered. Specifically, the dephasing rate due to an Ohmic bath of phonons is^{47,56} $\gamma_{\phi} \propto \alpha(\varepsilon_{13}^{\text{ld}})^2 k_B T / \Delta^2$, with $\Delta = \sqrt{(\varepsilon_{13}^{\text{ld}})^2 + 4(t_{13}^{\text{ld}})^2}$ and α is the strength of the electron-phonon interaction.

In general, the ratio of the current for a DQD with and without dephasing, Eqs. (D2) and (D1) respectively, has the ex-

pression $I_{\phi}^{\text{ld}}/I^{\text{ld}}$ obtained for the full TQD in the regime $\varepsilon \gg t_c$ with $\Gamma_D \lesssim t_c$ and $\gamma = 0$. This is shown in Fig. 6 in the form of the ratio I^{ld}/I , which tends to unity as the detuning ε increases, thereby demonstrating the validity of the effective description.

The fact that long-distance tunnelling in the full TQD appears only for moderate coupling to the drain can also be understood with the help of the effective model in (14): Large values of Γ_D induce a broadening of level $|3\rangle$ that may result in a substantial overlap with the detuned level $|2\rangle$, rendering the description in terms of an effective DQD invalid. From a dynamical point of view, strong coupling to the drain takes the effective DQD into a Zeno-like regime, in which the observation of the QD3 tends to freeze the charge mainly in QD1. This Zeno-like localization becomes dominant once we leave the regime of moderate coupling $\Gamma_D \sim t_c$, even for large detuning of QD2. It is also interesting that in this regime the Zeno effect reduces the only coherence participating in the effective DQD, ρ_{13}^s , [cf. Fig 3(b)] and therefore destroys the long-distance tunnelling in absence of dephasing.

We now turn to the analysis of the effect of dephasing on the transport properties of the effective DQD, i.e., we include the Lindblad term \mathcal{L}_{ϕ} of Eq. (3) with the effective rate γ^{ld} . We use the effective parameters for consistency with the main text, however the results are general for a DQD coupled to reservoirs and subjected to pure dephasing.

Applying the characteristic polynomial approach⁵⁰ we obtain the average current

$$I_{\phi}^{\text{ld}} = \frac{4\Gamma_S^{\text{ld}}\Gamma_D^{\text{ld}}\Gamma_{\phi}^{\text{ld}}(t_{13}^{\text{ld}})^2}{\Gamma_S^{\text{ld}}\Gamma_D^{\text{ld}}[(\Gamma_{\phi}^{\text{ld}})^2 + 4(\varepsilon_{13}^{\text{ld}})^2] + 4(t_{13}^{\text{ld}})^2\Gamma_{\phi}^{\text{ld}}(2\Gamma_S^{\text{ld}} + \Gamma_D^{\text{ld}})} \quad (\text{D2})$$

and the Fano factor

explicit form

$$\frac{I_{\phi}^{\text{ld}}}{I_0^{\text{ld}}} = \frac{\Gamma_{\phi}^{\text{ld}}[\Gamma_S^{\text{ld}}[(\Gamma_D^{\text{ld}})^2 + 4(\varepsilon_{13}^{\text{ld}})^2] + 4(t_{13}^{\text{ld}})^2(2\Gamma_S^{\text{ld}} + \Gamma_D^{\text{ld}})]}{\Gamma_S^{\text{ld}}\Gamma_D^{\text{ld}}[(\Gamma_{\phi}^{\text{ld}})^2 + 4(\varepsilon_{13}^{\text{ld}})^2] + 4(t_{13}^{\text{ld}})^2\Gamma_{\phi}^{\text{ld}}(2\Gamma_S^{\text{ld}} + \Gamma_D^{\text{ld}})}. \quad (\text{D4})$$

Note that for the full TQD system we assumed that QD1 and QD3 are in resonance, i.e., $\varepsilon_{13}^{\text{ld}} = 0$. Accordingly, Eq. (D4) reduces to Eq. (15) in the main text, which demonstrates that pure dephasing suppresses the current across a DQD at zero detuning.

¹ H. Lee, Y.-C. Cheng, and G. R. Fleming, *Science* **316**, 1462 (2007).

² V. I. Prokhorenko, A. R. Holzwarth, F. R. Nowak, and T. J. Aartsma, *J. Chem. Phys. B* **106**, 9923 (2002).

³ G. S. Engel, T. R. Calhoun, E. L. Read, T.-K. Ahn, T. Mančal, Y.-C. Cheng, R. E. Blankenship, and G. R. Fleming, *Nature* **446**, 782 (2007).

⁴ M. Mohseni, P. Rebentrost, S. Lloyd, and A. Aspuru-Guzik, *J.*

- Chem. Phys. **129**, 174106 (2008).
- ⁵ M. B. Plenio and S. F. Huelga, *New J. Phys.* **10**, 113019 (2008).
 - ⁶ F. Caruso, A. W. Chin, A. Datta, S. F. Huelga, and M. B. Plenio, *J. Chem. Phys.* **131**, 105106 (2009).
 - ⁷ S. F. Huelga and M. B. Plenio, *Contemp. Phys.* **54**, 181 (2013).
 - ⁸ F. Caruso, N. Spagnolo, C. Vitelli, F. Sciarrino, and M. B. Plenio, *Phys. Rev. A* **83**, 013811 (2011).
 - ⁹ F. Caruso, S. F. Huelga, and M. B. Plenio, *Phys. Rev. Lett.* **105**, 190501 (2010).
 - ¹⁰ A. Bermudez, M. Bruderer, and M. B. Plenio, *Phys. Rev. Lett.* **111**, 040601 (2013).
 - ¹¹ J. J. Mendoza-Arenas, T. Grujic, D. Jaksch, and S. R. Clark, *Phys. Rev. B* **87**, 235130 (2013).
 - ¹² J. J. Mendoza-Arenas, M. T. Mitchison, S. R. Clark, J. Prior, D. Jaksch, and M. B. Plenio, *New J. Phys.* **16**, 053016 (2014).
 - ¹³ S. A. Gurvitz, *Phys. Rev. B* **57**, 6602 (1998).
 - ¹⁴ Y. N. Chen, T. Brandes, C. M. Li, and D. S. Chuu, *Phys. Rev. B* **69**, 245323 (2004).
 - ¹⁵ B. Michaelis, C. Emary, and C. W. J. Beenakker, *Europhys. Lett.* **73**, 677 (2006).
 - ¹⁶ A. W. Chin, A. Datta, F. Caruso, S. F. Huelga, and M. B. Plenio, *New J. Phys.* **12**, 065002 (2010).
 - ¹⁷ R. Sánchez, F. Gallego-Marcos, and G. Platero, *Phys. Rev. B* **89**, 161402(R) (2014).
 - ¹⁸ C. W. Groth, B. Michaelis, and C. W. J. Beenakker, *Phys. Rev. B* **74**, 125315 (2006).
 - ¹⁹ C. Pörtl, C. Emary, and T. Brandes, *Phys. Rev. B* **80**, 115313 (2009).
 - ²⁰ F. Dominguez, S. Kohler, and G. Platero, *Phys. Rev. B* **83**, 235319 (2011).
 - ²¹ L. Gaudreau, S. A. Studenikin, A. S. Sachrajda, P. Zawadzki, A. Kam, J. Lapointe, M. Korkusinski, and P. Hawrylak, *Phys. Rev. Lett.* **97**, 036807 (2006).
 - ²² D. Schröer, A. D. Greentree, L. Gaudreau, K. Eberl, L. C. L. Hollenberg, J. P. Kotthaus, and S. Ludwig, *Phys. Rev. B* **76**, 075306 (2007).
 - ²³ L. Gaudreau, A. Kam, G. Granger, S. A. Studenikin, P. Zawadzki, and A. S. Sachrajda, *Appl. Phys. Lett.* **95**, 193101 (2009).
 - ²⁴ M. C. Rogge and R. J. Haug, *New J. Phys.* **11**, 113037 (2009).
 - ²⁵ G. Granger, L. Gaudreau, A. Kam, M. Pioro-Ladrière, S. A. Studenikin, Z. R. Wasilewski, P. Zawadzki, and A. S. Sachrajda, *Phys. Rev. B* **82**, 075304 (2010).
 - ²⁶ S. Amaha, W. Izumida, T. Hatano, S. Teraoka, S. Tarucha, A. Gupta, and D. G. Austing, *Phys. Rev. Lett.* **110**, 016803 (2013).
 - ²⁷ L. Gaudreau, G. Granger, A. Kam, G. C. Aers, S. A. Studenikin, P. Zawadzki, M. Pioro-Ladrière, and A. S. Wasilewski, Z. R. Sachrajda, *Nature Phys.* **8**, 54 (2012).
 - ²⁸ D. S. Saraga and D. Loss, *Phys. Rev. Lett.* **90**, 166803 (2003).
 - ²⁹ K. Kuzmenko, K. Kikoin, and Y. Avishai, *Phys. Rev. Lett.* **96**, 046601 (2006).
 - ³⁰ M. C. Rogge and R. J. Haug, *Phys. Rev. B* **77**, 193306 (2008).
 - ³¹ M. Seo, H. K. Choi, S.-Y. Lee, N. Kim, Y. Chung, H.-S. Sim, V. Umansky, and D. Mahalu, *Phys. Rev. Lett.* **110**, 046803 (2013).
 - ³² F. R. Braakman, P. Barthelemy, C. Reichl, W. Wegscheider, and L. M. K. Vandersypen, *Appl. Phys. Lett.* **102**, 112110 (2013).
 - ³³ J. Villavicencio, I. Maldonado, E. Cota, and G. Platero, *Phys. Rev. B* **88**, 245305 (2013).
 - ³⁴ M. Busl, G. Granger, L. Gaudreau, R. Sánchez, A. Kam, M. Pioro-Ladrière, S. A. Studenikin, P. Zawadzki, Z. R. Wasilewski, A. S. Sachrajda, and G. Platero, *Nat. Nanotech.* **8**, 261 (2013).
 - ³⁵ F. R. Braakman, P. Barthelemy, C. Reichl, W. Wegscheider, and L. M. K. Vandersypen, *Nat. Nanotech.* **8**, 432 (2013).
 - ³⁶ R. Sánchez, G. Granger, L. Gaudreau, A. Kam, M. Pioro-Ladrière, S. A. Studenikin, P. Zawadzki, A. S. Sachrajda, and G. Platero, *Phys. Rev. Lett.* **112**, 176803 (2014).
 - ³⁷ T. Hayashi, T. Fujisawa, H. D. Cheong, Y. H. Jeong, and Y. Hirayama, *Phys. Rev. Lett.* **91**, 226804 (2003).
 - ³⁸ T. Itakura and Y. Tokura, *Phys. Rev. B* **67**, 195320 (2003).
 - ³⁹ T. Fujisawa, T. Hayashi, and S. Sasaki, *Rep. Prog. Phys.* **69**, 759 (2006).
 - ⁴⁰ L. Fedichkin and A. Fedorov, *Phys. Rev. A* **69**, 032311 (2004).
 - ⁴¹ L. Fedichkin and A. Fedorov, *IEEE Trans. Nanotech.* **4**, 65 (2005).
 - ⁴² V. N. Stavrou and X. Hu, *Phys. Rev. B* **72**, 075362 (2005).
 - ⁴³ M. Field, C. G. Smith, M. Pepper, D. A. Ritchie, J. E. F. Frost, G. A. C. Jones, and D. G. Hasko, *Phys. Rev. Lett.* **70**, 1311 (1993).
 - ⁴⁴ Y. Levinson, *Europhys. Lett.* **39**, 299 (1997).
 - ⁴⁵ S. A. Gurvitz, *Phys. Rev. B* **56**, 15215 (1997).
 - ⁴⁶ Z.-Z. Li, C.-H. Lam, T. Yu, and J. Q. You, *Sci. Rep.* **3** (2013).
 - ⁴⁷ T. Brandes, *Phys. Rep.* **408**, 315 (2005).
 - ⁴⁸ H. P. Breuer and F. Petruccione, *The Theory of open quantum systems* (Oxford University Press, UK, 2002).
 - ⁴⁹ A. Rivas and S. F. Huelga, *Open quantum systems. An Introduction* (Springer, Heidelberg, 2012).
 - ⁵⁰ M. Bruderer, L. D. Contreras-Pulido, M. Thaller, L. Sironi, D. Obreschkow, and M. B. Plenio, *New J. Phys.* **16**, 033030 (2014).
 - ⁵¹ T. Baumgratz, M. Cramer, and M. B. Plenio, arXiv preprint arXiv:1311.0275 (2013).
 - ⁵² P. Facchi and S. Pascazio, “Unstable systems and quantum Zeno phenomena in quantum field theory,” in *Fundamental Aspects of Quantum Physics* (World Scientific, 2003) Chap. 13, p. 222.
 - ⁵³ P. Facchi, G. Marmo, and S. Pascazio, *J. Phys.: Conf. Ser.* **196**, 012017 (2009).
 - ⁵⁴ V. Paulisch, H. Rui, H. K. Ng, and B.-G. Englert, *Eur. Phys. J. Plus* **129**, 12 (2014).
 - ⁵⁵ T. H. Stoof and Y. Nazarov, *Phys. Rev. B* **53**, 1050 (1996).
 - ⁵⁶ R. Aguado and T. Brandes, *Phys. Rev. Lett.* **92**, 206601 (2004).